Anomalous Phosphorescence from an Organometallic White-Light Phosphor

Lopa Paul,[1] *Swapan Chakrabarti,*[1,*] *and Kenneth Ruud.*[2,*]

[1]Department of Chemistry, University of Calcutta

92, A.P.C.Ray Road, Kolkata 700 009

India

[2]Hylleraas Centre for Quantum Molecular Sciences, Department of Chemistry, University of Tromsø - The Arctic University of Norway,

N-9037 Tromsø, Norway

AUTHOR INFORMATION

Corresponding Author

*E-mail: swcchem@caluniv.ac.in Fax: 91-33-23519755

*E-mail: kenneth.ruud@uit.no

ABSTRACT: We report theoretical results on the possible violation of Kasha's rule in the phosphorescence process of (acetylacetonato)bis(1-methyl-2-phenylimidazole)iridium(III), and show that the anomalous emission from both the T_1 and T_2 states is key to its white-light phosphorescence. This analysis is supported by the calculated Boltzmann-averaged phosphorescence lifetime of 2.21 μs, estimated including both radiative and nonradiative processes and in excellent agreement with the experimentally reported value of 1.96 ± 0.1 μs. The T_2 state is found to be of metal-to-ligand charge transfer character (dπ→nπ) and the d orbital contribution comes from $5d_z^2$ and $5d_{x^2-y^2}$, whereas the S_1 and T_1 states both have dπ-pπ character with significant $5d_{xz}$ orbital contribution, allowing for efficient intersystem crossing from the S_1 to the T_2 state, and in turn phosphorescence from the T_2 state. Our results open new opportunities for tailoring the phosphorescence wavelength and thus the design of molecules with improved photovoltaic properties.

TOC GRAPHICS

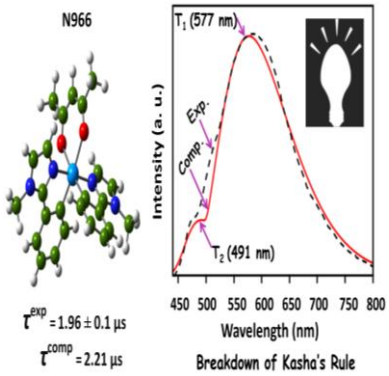

According to Kasha's rule, fluorescence and phosphorescence will in general be observed from the S_1 and T_1 states , respectively. However, Beer and Longuet-Higgins observed the first breakdown of Kasha's rule in 1955 while investigating the fluorescence spectrum of an aromatic molecule, azulene.[1] At present, molecules showing such unusual fluorescence from higher excited singlet states are not uncommon.[2-6] In contrast, phosphorescence analogs showing emission from higher triplet states are very rare. Historically, the breakdown of Kasha's rule in phosphorescence was first observed in p-benzoquinone by Itoh *et al.*[7-11] Since then, this phenomenon has only been observed in a fullerene (C_{70})[7,12] and eight other pure organic molecules.[7] Finding inorganic materials or organometallic complexes that display anomalous phosphorescence is made difficult by the often strong spin-orbit coupling between the S_0 and T_1 states and the often small energy gap between the T_1 and T_2 states, both effects that will favor normal phosphorescence from the T_1 state.

Experimentally, it has been observed that a white light phosphorescent organometallic complex, (acetylacetonato)bis(1-methyl-2-phenylimidazole)iridium(III) popularly known as N966, had a broad emission spectrum in CH_2Cl_2 solution at 298K, covering the spectral range from 440 to 800 nm.[13] Careful examination of this solution-phase emission spectrum also reveals the existence of a shoulder at 475 nm which is even more conspicuous in the electro-phosphorescence spectrum and low temperature (77 K) emission spectrum of this material, indicating a possible violation of Kasha's rule in this organometallic complex. This unusual spectral feature of N966 led us to study its phosphorescence spectrum using first-principles calculations. To explain the photophysical origin of this anomalous phosphorescence spectrum, we have performed time-dependent density functional theory based response theory (TDDFT-RT)[14-17] calculations and evaluated both the Franck-Condon and Herzberg-Teller contributions to

the radiative lifetime. The explicit quantitative evaluations of the nonradiative and intersystem crossing rates have also been carried out involving both the T_1 and T_2 states, contributing to the understanding of the mechanism of unusual phosphorescence from this organometallic complex.

The structure of the N966 complex is shown in Figure 1. The ground-state (S_0) and the lowest excited triplet state (T_1) of N966 were optimized using density functional theory with the latter state having been optimized from the S_0 geometry applying an unrestricted approach. The lowest excited singlet state (S_1) and the second lowest triplet state (T_2) structures were optimized from the electron density of the S_0 state using excited-state gradients obtained using TD-DFT.[18] All optimizations were carried at the B3LYP/cc-pVDZ level of theory, using for iridium the LANL2DZ basis set and its corresponding pseudopotential to incorporate scalar-relativistic effects on the core electrons of iridium. Harmonic vibrational frequencies were calculated at the optimized geometries to verify that the structures correspond to energy minima. The minimum-energy structure of S_0 has C_2 symmetry, the symmetry axis bisecting the acetylacetonato (acac) group. The C_2 symmetry is retained for the optimized structures of the S_1 and T_2 states, whereas all symmetry is lost in the T_1 excited state. The bond lengths between the central atom and all atoms directly linked to it for the different states are collected in the Supporting Information, Table S1. The absorption calculations have been performed at the optimized structure of the electronic ground state and the details of these calculations are presented in the Supporting Information. All calculations were performed with the Gaussian 09 program.[19]

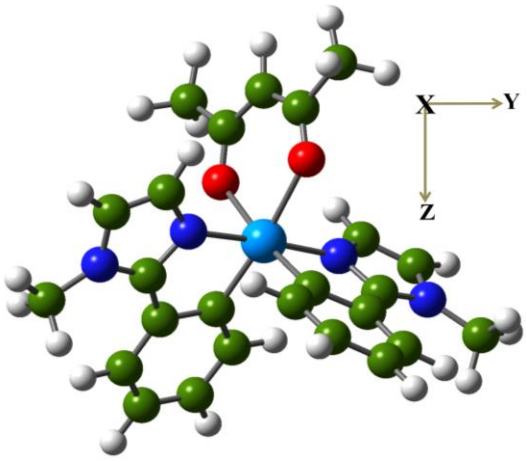

Figure 1. Optimized, ground-state structure of (acetylacetonato)bis(1-methyl-2-phenylimidazole)iridium(III) [($C_{25}H_{25}IrN_4O_2$)]. Different colors represent different atoms - red for oxygen, green for carbon, deep blue for nitrogen, light blue for iridium and grey for hydrogen.

The experimental findings suggest that the phosphorescence spectrum of N966 covers the entire visible region (440-800 nm), with the maximum at 570 nm. From TDDFT-RT calculations, we find the T_1 emission to occur at 577 nm, in excellent agreement with the experimental results. It is to be noted that the TDDFT-RT calculation is based on the electronic states only, and as a result, this theory alone cannot shed light on the origin of this extremely broad band. Bolink *et al.*[13] did not address this issue, though they suggested that vibronic coupling[20,21] between the T_1 and S_0 states could be a possible reason behind the large spectral broadening. To verify the role of vibronic coupling, we have calculated the FC overlap integral involving all the normal modes of the molecule. The detailed computational procedure is given in the method section. The FC vibronic spectrum with the vibrational progression of the T_1 state is presented in Figure 2a and the figure illustrates that vibronic effects in the T_1 state make a significant contribution to the broadening of the spectrum in the green and red region. However, the vibronic emission

spectrum of T_1 is unable to provide any satisfactory explanation for the existence of a shoulder in the lower wavelength region (475 nm). Being blue-shifted by 3523 cm^{-1} from the major peak at 577 nm, the shoulder could neither be a vibrationally resolved component as this always occurs with a bathochromic shift, nor be the contribution of a triplet sublevel because the calculated zero field splitting is only -46 cm^{-1} (a negative ZFS parameter indicates prolate electron distribution, i.e. an elongation in one direction). It has previously been observed that the presence of molecular oxygen in the triplet state interferes with the emission spectrum as noise.[7] However, the chance of this shoulder being the result of such solvent-trapped molecular oxygen is very unlikely because molecular oxygen shows emission at different wavelengths: the phosphorescence occurs at 1270 nm whereas the fluorescence is observed within the wavelength range of 195-260 nm. Moreover, the intensity of this shoulder is visibly much larger in the N966-based solid state diode (where no oxygen is present) and in the emission spectrum recorded at 77 K as well. This compelled us to consider the possible involvement of a higher excited triplet state in the overall phosphorescence of N966. Indeed, the TDDFT-RT computed phosphorescence wavelength of T_2, 491 nm, is just 16 nm red-shifted from the position of the shoulder of the experimentally recorded phosphorescence spectra (Figure 2b). Figure 2b also shows that the vibronic contribution of T_2 is very small compared to that of the T_1 state. The complete phosphorescence spectrum simulated with full width half-maximum (FWHM) = 2000 cm^{-1} (0.24 eV) together with the experimental spectrum is presented in Figure 2c, which shows a nice agreement, indicating that the T_2 contribution to the phosphorescence cannot be ruled out.

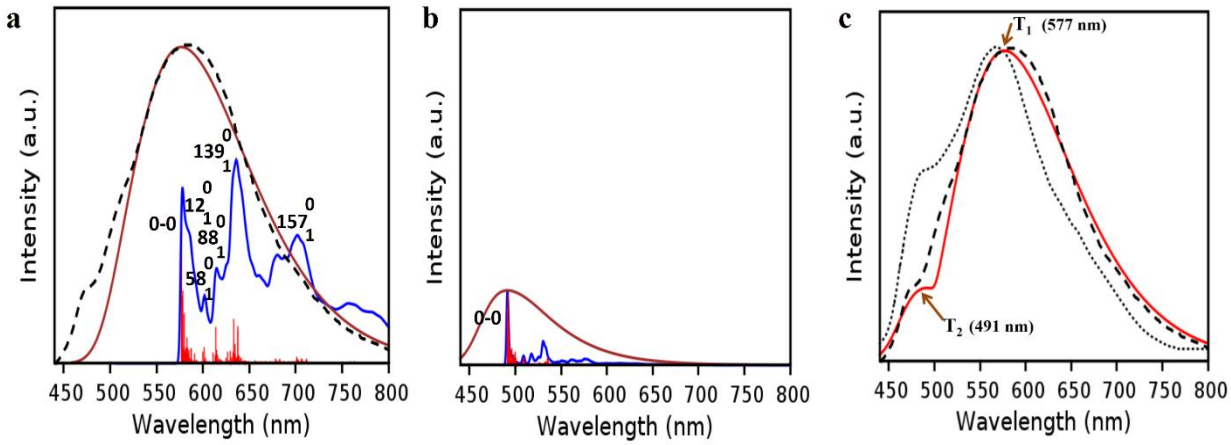

Figure 2. (a)Vibrationally resolved simulated spectrum with FWHM = 2000 cm^{-1} (brown), FWHM = 100 cm^{-1} (blue) and stick-spectrum (red) of the T_1 state indicating the five most active vibrational modes other than the 0–0 transition together with the experimental photophosphorescence spectrum (dashed line). (b)Vibrationally resolved simulated spectrum with FWHM = 2000 cm^{-1}(brown), FWHM = 100 cm^{-1} (blue) and stick-spectrum (red) of the T_2 state showing the 0–0 vibrational mode. (c) Experimental photophosphorescence (dashed line), electrophosphorescence (dotted line) and simulated total phosphorescence [with FWHM = 2000 cm^{-1}(red line)] spectra of N966. The electrophosphorescence spectrum shows a prominent shoulder in the higher-energy region (~ 485 nm), while experimental photophosphorescence showed the shoulder at 476 nm, and both spectra show a broad peak at 570 nm.

Phosphorescence from a higher triplet state (T_2) has been observed in some aromatic molecules and has been attributed to the thermal activation from T_1 due to the small energy gap between the two triplet states (~ 200 – 450 cm^{-1}).[7] However, in the present case, the energy gap between T_1 and T_2 is considerably higher (3029 cm^{-1}) and at room temperature the Boltzmann population ratio is approximately 4.9 $x10^{-7}$, indicating that population of the T_2 state by thermal activation from T_1 cannot alone give efficient phosphorescence from T_2, rather the population of the T_2

state is due to non-radiative processes. We nevertheless assume that two triplet states are in thermal equilibrium, as previously observed in 9,10-Phenanthrenequinone.[22]

After excitation, the most crucial step towards the commencement of phosphorescence is the intersystem crossing (ISC) and, depending on the energy gap and the strength of the spin-orbit interaction,[23-25] ISC could take place between S_1-T_1 or even with higher triplet states. In the present case, the calculated $\Delta E_{S_1\text{-}T_1}$ and $\Delta E_{S_1\text{-}T_2}$ are 0.7 eV are 0.3 eV, respectively, and the spin-orbit interaction between the S_1-T_2 (513 cm^{-1}) is significantly larger than S_1-T_1 (93 cm^{-1}), indicating that both factors will favor efficient ISC from S_1 to T_2. It is well known that ISC is a complex process that involves dynamic reorganization of one state to the other, where molecular vibrations and vibrational density of states could alter the ISC rate constant (k_{ISC}) considerably. To evaluate k_{ISC}, we use Marcus-Levich-Jortner theory[26] derived in the framework of Fermi's golden rule, and the rate constant is then expressed as[27,28]

$$k_{ISC} = \frac{2\pi}{\hbar}\langle T_n | H_{SOC} | S_1 \rangle^2 \times \text{FCWD} \qquad (1)$$

where the first term is the square of the spin-orbit coupling (SOC) matrix element and the second term gives the Franck–Condon-weighted density of states (FCWD). The details of this expression are given in the Supplementary Information. The k_{ISC} achieved for S_1-T_1 and S_1-T_2 are 3.95×10^{11} s^{-1} and 5.29×10^{11} s^{-1}, respectively, where the latter is 1.3 times higher than the former and the results suggests that T_2 is gaining more population from S_1 than the T_1 state. It is worth noting that albeit the square of the SOC value for $S_1 \rightarrow T_2$ is almost 30 times greater than that of $S_1 \rightarrow T_1$, the calculated k_{ISC} of the former is only 1.3 times higher than the latter due to the FCWD. The FCWD depends on the dimensionless electron-phonon coupling strength (the Huang-Rhys factor (S)[29]) over all the normal modes and various energy parameters,

reorganization energy, normal mode frequency and the energy difference between the states of interest, as can be seen from Eq S2 provided in the Supporting Information. Because the energy parameter displays an exponential decaying contribution to the FCWD, the contribution of the energy term of the FCWD to the $S_1 \rightarrow T_2$ transition is only 1.6 times larger than for the $S_1 \rightarrow T_1$ transition, giving a clear indication that the Huang-Rhys factor plays the decisive role in tuning the k_{ISC} values. The Huang-Rhys factor for the $S_1 \rightarrow T_1$ and $S_1 \rightarrow T_2$ transitions are 7.35 and 13.97, respectively, which matches well the corresponding 0-0 overlap values of 1.29×10^{-2} and 3.98×10^{-4}. Incorporating the Huang-Rhys factor in Eq S2 (Supporting Information) yields FCWD values of 0.300 eV^{-1} and 0.014 eV^{-1} for the $S_1 \rightarrow T_1$ and $S_1 \rightarrow T_2$ transitions, respectively, and the ratio of the FCWD of the former to the latter is almost 21, thus cancelling the difference in SOC which otherwise strongly favors the $S_1 \rightarrow T_2$ transition.

Although the differences are small, the relatively faster ISC between S_1-T_2 compared to S_1-T_1 requires a more detailed analysis, and we have therefore inspected the nature of the frontier molecular orbitals of the relevant states as shown in Figure 3. Interestingly, the $S_1 \rightarrow T_1$ transition is of $^1[d\pi\text{-}p\pi]^* \rightarrow {}^3[d\pi\text{-}p\pi]^*$ type, whereas the $S_1 \rightarrow T_2$ transition involves $^1[d\pi\text{-}p\pi]^* \rightarrow {}^3[d\pi\text{-}p\pi\text{-}n\pi]^*$ orbitals due to charge transfer from the 5d orbital of iridium to the acac moiety. The population analysis suggests that the major d orbital contribution to the LUMO comes from the $5d_{xz}$ orbital, whereas both the $5d_z^2$ and $5d_{x^2-y^2}$ have participated in the formation of LUMO+1. The small energy gap between the S_1 and T_2 states together with efficient spin orbit coupling will make k_{ISC} larger than that of S_1 and T_1. Moreover, the presence of a larger non-bonded electron density at the oxygen atom in the LUMO +1 orbital will also lead to an enhancement of the SOC vis-à-vis efficient ISC between the S_1 and T_2 states.[30]

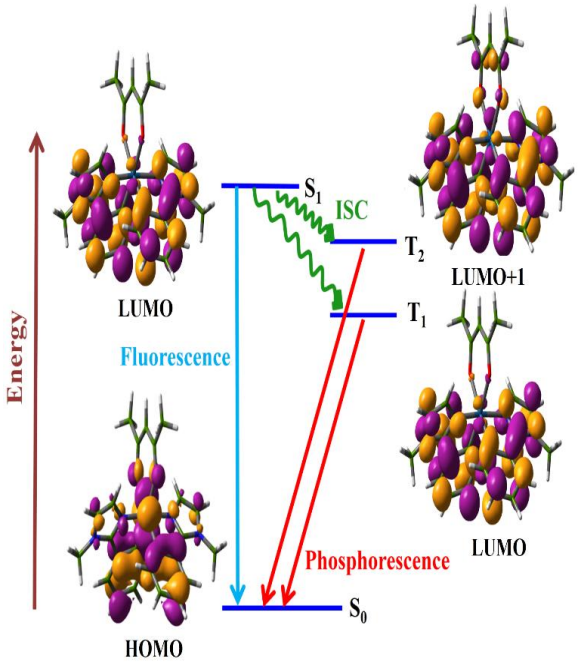

Figure 3. Schematic representation showing the TD-DFT calculated energy levels, frontier molecular orbitals (FMO's) (isovalue = 0.03) involved in the transitions to the singlet (S_0 and S_1) and triplet (T_1 and T_2) states of N966. The $T_1 \rightarrow S_0$ and $T_2 \rightarrow S_0$ transitions are assigned to LMCT [$\pi_{cml}^* \rightarrow d$] (cml refers to the cyclometallated ligand) and LMCT [$\pi_{acac}^* \rightarrow d$], respectively. $\Delta E_{S_1 \rightarrow S_0} = 2.83$eV, $\Delta E_{T_1 \rightarrow S_0} = 2.15$eV and $\Delta E_{T_2 \rightarrow S_0} = 2.49$eV.

To strengthen our arguments further, we have computed both the radiative and nonradiative lifetimes explicitly. The net lifetime is defined as $\tau = (k_r + k_{nr})^{-1}$, where k_r and k_{nr} are the radiative and nonradiative rate constants, respectively. For evaluating k_r, we have adopted the high-temperature limit approximation[31] where all three sublevels of the triplet manifold participate equally in the phosphorescence process, and the relevant expression is given in the Supporting Information. In addition, the 0-0 FC overlap integrals are taken into account in the computation of the phosphorescence transition moments because vibronic coupling is of fundamental importance in this system. Moreover, using the refractive index of CH_2Cl_2 as 1.424, the

Strickler-Berg correction[32] has also been applied to the FC-weighted rate constant. The rate constant calculated including all possible corrections, together with the radiative lifetime (τ^{rad}), are presented in Table 1.

Table1. Electronic transition, transition energy [E (eV)], rate constant for pure electronic transition [k_{elec} (s^{-1})], FC weighted rate constant [$k^{0\text{-}0}$ (s^{-1})], Strickler-Berg corrected rate constant [$k^{0\text{-}0,SB}$ (s^{-1})], radiative lifetime [τ^{rad} (μs)] and the total computed lifetime [τ_n^{comp} (μs)] of N966.

$T_n \rightarrow S_0$	Medium	E	k_{elec}	$k^{0\text{-}0}$	$k^{0\text{-}0,SB}$	τ^{rad}	τ_n^{comp}
n=1	Gas-phase	2.149	2.29×10^4	4.58×10^2	-	2182.69	~1.67
	Solvent-phase	2.169	2.77×10^4	5.52×10^2	1.12×10^3	892.93	
n=2	Gas-phase	2.523	9.11×10^4	2.30×10^4	-	43.37	~3.32
	Solvent-phase	2.547	1.00×10^5	2.54×10^4	5.16×10^4	19.37	

From Table 1, it is clear that the radiative lifetime from T_1 is almost 1000 times longer than that observed experimentally, whereas the lifetime of the T_2 state is only 10 times longer. In a recent work, Paul *et al.*[33] showed that inclusion of the FC factor alone fails to explain the vibronic phosphorescence lifetime of an organic dimer and it was further demonstrated that the displacement-induced vibronic phosphorescence transition moment arising from the Herzberg-Teller (HT) contribution[34] along the normal modes are responsible for the ultralong lifetime of this class of aggregated organic phosphors. The HT contribution listing all the 0-1 bands of selected normal modes and the corresponding method of calculation are provided in the Supporting Information. The k_r and τ^{rad} obtained from the HT term are 5.60×10^2 s^{-1} and ~ 1.78 ms, respectively, for the T_1 state, and in contradiction with the experimental results. We did not perform HT calculations on the T_2 state because the vibronic feature of the T_2 state is relatively

weak. This makes it clear that k_{nr} is the dominant contribution to the lifetime of both states, and in particular for the T_1 state, in agreement with the experimental report, suggesting very low photoluminescence quantum yield (PLQY=0.015), where PLQY = k_r / (k_r + k_{nr}). Within the limitations of the FC approximation in the non-adiabatic scheme, the k_{nr} of the $T_n \rightarrow S_0$ transition is evaluated by the same expression as shown in Eq 1. As for k_r, k_{nr} also involves the evaluation of SOC integrals, namely $\langle T_n|H_{SO}|S_0\rangle$, where we have used the full one- and two- electron Breit–Pauli SO operator as implemented in Dalton,[35,36] whereas the FCWD was estimated following the approach used for k_{ISC}. The calculated nonradiative rate constant (k_{nr}) for T_1 is 5.98 $\times 10^5$ s^{-1}, 100-1000 times higher than that of k_r, leading to a net lifetime of ~ 1.67 μs as (see Table 1). k_{nr} for T_2 is 2.64 $\times 10^5$ s^{-1}, and the corresponding net lifetime is ~ 3.32 μs (Table 1). Due to thermal equilibrium, the lifetime of N966 would be the inverse of the Boltzmann-averaged total rate constant of the two lower-lying triplet states[37] and according to our calculation, the lifetime will be 2.21 μs, in good agreement with the experimental value of (1.96 ± 0.1 μs).[13] The lifetime calculations thus lend support to our proposal that both the T_1 and T_2 states contribute to the net phosphorescence of N966.

In conclusion, we have established that a breakdown of Kasha's rule occurs in the phosphorescence of the complex N966, and this is the first observation of this kind for an organometallic phosphor material. We have demonstrated that vibronic phosphorescence from the T_1 state gives spectral broadening in the green and red region, whereas electronic phosphorescence from the T_2 state is the origin of the blue region of the spectrum. The significant involvement of T_2 is supported by the more efficient intersystem crossing between the S_1 and T_2 states compared to that between S_1 and T_1. Calculations of lifetimes involving both radiative and nonradiative processes also indicate that the experimental lifetime is due to the

Boltzmann averaged phosphorescence from both the T_1 and T_2 states. Finally, we think that our findings will motivate experimentalists to benchmark these calculated data by performing optically detected magnetic resonance experiment at 4.2 K.

ASSOCIATED CONTENT

Supporting Information.

The Supporting information is available free of charge.

(1) Computational details. (2) Co-ordinates of the optimized geometries of N966. (3) Structural parameters. (4) One photon absorption (OPA). (5) Calculation of Franck-Condon (FC) integrals. (6) Estimation of the rate constant for intersystem crossing (ISC) [k_{ISC}]. (7) Expression for the radiative rate constant (k_r) for pure electronic transitions. (8) Herzberg-Teller (HT) contributions to k_r for $S_0 \rightarrow T_1$ transitions. (PDF)

AUTHOR INFORMATION

Notes

The authors declare no competing financial interests.

ACKNOWLEDGMENT

L.P. thanks the Council of Scientific and Industrial Research (CSIR) for granting her the Senior Research Fellowship.

REFERENCES

(1) Beer, M.; Longuet-Higgins, H. C. Anomalous Light Emission of Azulene. *J.Chem.Phys.***1955**, *23*, 1390-1391.

(2) Qian, H.; Cousins, M. E.; Horak, E. H.; Wakefield, A.; Liptak, M. D.; Aprahamian, I. Suppression of Kasha's Rule as a Mechanism for Fluorescent Molecular Rotors and Aggregation-Induced Emission. *Nat. Chem.* **2016**, *9*, 83-87.

(3) Yushchenko, O.; Licari, G.; Mosquera-Vazquez, S.; Sakai, N.; Matile, S.; Vauthey, E.; Ultrafast Intersystem-Crossing Dynamics and Breakdown of the Kasha-Vavilov'sRule of Naphthalenediimides. *J. Phys. Chem. Lett.* **2015**, *6*, 2096-2100.

(4) Choi, C. L.; Li, H.; Olson, A. C. K.; Jain, P. K.; Sivasankar, S.; Alivisatos, A. P. Spatially Indirect Emission in a Luminescent NanocrystalMolecule. *Nano Lett.* **2011**, *11*, 2358-2362.

(5) Brancato, G.; Signore, G.; Neyroz, P.; Polli, D.; Cerullo, G.; Abbandonato, G.; Nucara, L.; Barone, V.; Beltram, F.; Bizzarri. R. Dual Fluorescence Through Kasha's Rule Breaking: An Unconventional Photo Mechanism for Intracellular Probe Design. *J. Phys. Chem. B* **2015**, *119*, 6144-6154.

(6) Yanagi, K.; Kataura, H. Breaking Kasha's Rule. *Nat. Photonics* **2010**, *4*, 200-20.

(7) Itoh, T. Fluorescence and Phosphorescence from Higher Excited States of Organic Molecules. *Chem. Rev.* **2012**, *112*, 4541-4568.

(8) Goodman, J.; Brus, L. E. Distant Intramolecular Interaction Between Identical Chromophores: The n-π* Excited State of p-Benzoquinone. *J. Chem. Phys.* **1978**, *69*, 1604.

(9) Itoh, T.; Hashimoto, R. J. Temperature Dependence of the Emission Spectra of p-Benzoquinone in a p-Dichlorobenzene Matrix. *J. Lumin.* **2012**, *132*, 236-239.

(10) Itoh, T. Emission Spectrum of p-Benzoquinone in a Fluid Solution. *Spectrochim. Acta, A* **1984**, *40*, 387-389.

(11) Khalil, O. S.; Goodman, L. J. Characterization of the Anomalous Phosphorescence of p-Chlorobenzaldehyde in Polycrystalline Methylcyclohexane at 4.2 K. *J. Am. Chem. Soc.* **1977**, *99*, 5924-5931.

(12) Rice, J. H.; Galaup, J.-P.; Leach, S. Fluorescence and Phosphorescence Spectroscopy of C 70 in Toluene at 5 K: Site Dependent Low Lying Excited States. *Chem. Phys.* **2002**, *279*, 23-41.

(13) Bolink, H. J.; Angelis, F. D.; Baranoff, E.; Klein, C.; Fantacci, S.; Coronado, E.; Sessolo, M.; Kalyansundaram, K.; Gratzel, M.; Nazeeruddin, M. K.White-Light Phosphorescence Emission from a Single Molecule: Application to OLED. *Chem. Commun.* **2009**, 4672-4674.

(14) Hettema, H.; Jensen, H. J.; Jørgensen, P.; Olsen, J. Quadratic Response Functions for a Multiconfigurational Self-Consistent Field Wave Functions. *J. Chem. Phys.* **1992**, *97*, 1174-1190.

(15) Vahtras, O.; Ågren, H.; Jo/rgensen, P.; Jensen, H. J. A.; Helgaker, T.; Olsen, J. Multiconfigurational Quadratic Response Functions for Singlet and Triplet Perturbations: The Phosphorescence Lifetime of Formaldehyde. *J. Chem. Phys.* **1992**, *97*, 9178-9187.

(16) Runge, E.; Gross, E. K. U. Density-Functional Theory for Time-Dependent Systems. *Phys. Rev. Lett.* **1984**, *52*, 997-1000.

(17) Salek, P.; Vahtras, O.; Helgaker, T.; Ågren, H. Density-functional Theory of Linear and Nonlinear Time-Dependent Molecular Properties. *J. Chem. Phys.* **2002**, *117*, 9630-9645.

(18) Furche, F.; Ahlrichs, R. Adiabatic Time-Dependent Density Functional Methods for Excited State Properties. *J. Chem. Phys.* **2002**, *117*, 7433-7447.

(19) *GAUSSIAN 09*, revision D.01, Gaussian, Inc.: Wallingford, CT, 2009.

(20) Kleinschmidt, M.; Wüllen, C. V.; Marian, C. M. Intersystem-Crossing and Phosphorescence Rates in fac-$Ir^{III}(ppy)_3$: A Theoretical Study Involving Multi-Reference Configuration Interaction Wavefunctions. *J. Chem. Phys.* **2015**, *142*, 94301-94316.

(21) Marian, C. M. Spin-Orbit Coupling and Intersystem Crossing in Molecules. *WIREs Comput Mol Sci* **2012**, *2*, 187-203.

(22) Kumar, V. R.; Rajkumar, N.; Ariese. F.; Umapathy, S. Direct Observation of Thermal Equillibrium of Excited Triplet States of 9,10-Phenanthrenequinone. A Time-Resolved Resonance Raman Study. *J. Phys. Chem. A* **2015**, *119*, 10147-10157.

(23) Baryshnikov, G.; Minaev, B.; Ågren, H. Theory and Calculation of the Phosphorescence Phenomenon. *Chem. Rev.* **2017**, *117*, 6500-6537.

(24) Minaev, B.; Ågren, H.; Angelis, F. D. Theoretical Design of Phosphorescence Parameters for Organic Electro-Luminescence Devices Based on Iridium Complexes. *Chem. Phys.* **2009**, *358*, 245-257.

(25) Minaev, B.; Baryshnikov, G.; Ågren, H. Principles of Phosphorescent Organic Light Emitting Devices. *Phys. Chem. Chem. Phys.* **2014**, *16*, 1719-1758.

(26) Brédas, J. L.; Beljonne, D.; Coropceanu, V.; Cornil, J. Charge-Transfer and Energy-Transfer Processes in Pi-Conjugated Oligomers and Polymers: A Molecular Picture. *Chem. Rev.* **2004**, *104*, 4971-5003.

(27) Tong, G. S. M.; Chan, K. T.; Chang, X.; Che, C. Theoretical Studies on the Photophysical Properties of Luminescent Pinser Gold(III) Arylacetylide Complexes: The Role of π-Conjugation at the C-Deprotonated [C^N^C] Ligand. *Chem. Sci.* **2015**, *6*, 3026-3037.

(28) Schimdt, K. *et al.* Intersystem Crossing Processes in Nonplanar Aromatic Heterocyclic Molecules. *J. Phys. Chem. A* **2007**, *111*, 10490-10499.

(29) Jong, M. D.; Seijo, L.; Meijerink, A.; Rabouw, F. T. Resolving the Ambiguity in the Relation between Stokes Shift and Huang-Rhys Parameter. *Phys. Chem. Chem. Phys.* **2015**, *17*, 6959-16969.

(30) Li, E. Y.-T.; Jiang, T.-Y.; Chi, Y.; Chou, P.-T. Semi-Quantitative Assessment of the Intersystem Crossing Rate: An Extension of the El-Sayed Rule to the Emissive Transition Metal Complexes. *Phys. Chem. Chem. Phys.* **2014**, *16*, 26184-26192.

(31) Younker, J. M.; Dobbs, K. D. Correlating Experimental Photophysical Properties of Iridium(III) Complexes to Spin-Orbit Coupled TDDFT Predictions. *J. Phys. Chem. C* **2013**, *117*, 25714-25723.

(32) Mori, K.; Goumans, T. P. M.; Lenthe, E. V.; Wang, F. Predicting Phosphorescent Lifetimes and Zero-Field Splitting of Organometallic Complexes with Time-Dependent Density Functional Theory Including Spin-Orbit Coupling. *Phys. Chem. Chem. Phys.* **2014**, *16*, 14523-14530.

(33) Paul, L.; Chakrabarti, S.; Ruud, K. Origin of Dual-Peak Phosphorescence and Ultralong Lifetime of 4,6-Diethoxy-2-carbazolyl-1,3,5-triazine. *J. Phys. Chem. Lett.* **2017**, *8*, 1253-1258.

(34) Minaev, B. F.; Knuts, S.; Ågren, H.; Vahtras, O. The Vibronically Induced Phosphorescence in Benzene. *Chem. Phys.* **1993**, *175*, 245-254.

(35) Tunell, I.; Rinkevicius, Z.; Vahtras, O.; Salek, P.; Helgaker, T.; Ågren, H. Density Functional Theory of Nonlinear Triplet Response Properties with Applications to Phosphorescence. *J. Chem. Phys.* **2003**, *119*, 11024-11034.

(36) *DALTON, a Molecular Electronic Structure Program,* Release Dalton 2016.2 (2015), see http://daltonprogram.org. (15 Sep, 2017).

(37) Kühn, M.; Weigend, F. Phosphorescence Lifetimes of Organic Light-Emitting Diodes from Two-Component Time-Dependent Density Functional Theory. *J. Chem. Phys.* **2014**, *141*, 224302.